AGU PUBLICATIONS

Geophysical Research Letters

RESEARCH LETTER
10.1002/2014GL063003

Key Points:
- Global footprint of MIS3 ocean temperature anomalies to AMOC changes
- Combination of model results with SST records to estimate MIS3 AMOC changes
- About 10 Sv change in AMOC strength between stadial and interstadial states

Correspondence to:
X. Zhang,
xzhang@marum.de

Citation:
Zhang, X., M. Prange, U. Merkel, and M. Schulz (2015), Spatial fingerprint and magnitude of changes in the Atlantic meridional overturning circulation during marine isotope stage 3, *Geophys. Res. Lett.*, *42*, 1903–1911, doi:10.1002/2014GL063003.

Received 29 DEC 2014
Accepted 18 FEB 2015
Accepted article online 20 FEB 2015
Published online 24 MAR 2015

Spatial fingerprint and magnitude of changes in the Atlantic meridional overturning circulation during marine isotope stage 3

Xiao Zhang[1], Matthias Prange[1], Ute Merkel[1], and Michael Schulz[1]

[1]MARUM-Center for Marine Environmental Sciences and Faculty of Geosciences, University of Bremen, Bremen, Germany

Abstract Pronounced millennial-scale climate variability during marine isotope stage 3 (MIS3) is considered to be linked to changes in the state of the Atlantic meridional overturning circulation (AMOC), i.e., a warm interstadial/cold stadial state corresponds to a strong/weak AMOC. Based on a series of freshwater hosing/extraction experiments with the state-of-the-art Community Climate System Model version 3, we construct a global spatial fingerprint of oceanic temperature anomalies in response to AMOC changes under MIS3 boundary conditions. Highest sensitivity to AMOC changes, especially in summer, is found in northeastern North Atlantic sea surface temperature, but a characteristic temperature fingerprint is also found at subsurface levels. After testing significance of the linear sea surface temperature (SST)-AMOC regressions, the model results are combined with paleo-SST records to estimate the magnitude of millennial-scale Dansgaard-Oeschger AMOC variations during MIS3. The results suggest a mean difference in AMOC strength between interstadial and (non-Heinrich) stadial states of 9.2 ± 1.2 Sv (1σ).

1. Introduction

The Atlantic meridional overturning circulation (AMOC) is a major component of the global climate system regulating the distribution of heat as well as the cycling of carbon and other nutrients [e.g., *Ganachaud and Wunsch*, 2000; *Johns et al.*, 2011]. Due to its high relevance for the climate system, many studies attempted to quantify changes in AMOC strength during the last glacial and deglaciation based on proxy records and climate models [e.g., *LeGrand and Wunsch*, 1995; *Winguth et al.*, 2000; *Gebbie and Huybers*, 2006; *Lynch-Stieglitz et al.*, 2007; *Ritz et al.*, 2013]. Pronounced millennial-scale climate variability during marine isotope stage 3 (MIS3; 57–29 thousand years before present [ka B.P.]), characterized by transitions between cold stadials and warm interstadials at northern latitudes [*Dansgaard et al.*, 1993; *Bond et al.*, 1993] and termed Dansgaard-Oeschger (D-O) cycles, is most likely related to changes in AMOC strength [e.g., *Keigwin and Boyle*, 1999; *Broecker*, 2000; *Sarnthein et al.*, 2001; *Elliot et al.*, 2002; *Rahmstorf*, 2002; *EPICA Community Members*, 2006]. A warm interstadial state corresponds to a strong circulation, while a cold stadial state is characterized by a weak circulation. Probably the most dramatic disruptions of the glacial AMOC are associated with massive layers of ice-rafted debris in the North Atlantic during so-called Heinrich stadials [e.g., *Broecker et al.*, 1992; *Grousset et al.*, 1993; *Hemming*, 2004; *McManus et al.*, 2004].

Despite the importance of AMOC changes in shaping millennial-scale climate variability during MIS3, the magnitude of changes in circulation strength necessary to cause stadial-interstadial climate transitions is not known. Combining climate model simulations with marine proxy records, *Ritz et al.* [2013] recently presented an estimate for AMOC variations during the last deglaciation based on a linear relationship between Atlantic sea surface temperatures (SST) and AMOC strength. Their results suggest millennial-scale reductions in AMOC strength of ~14 Sv ($1\ \text{Sv} = 10^6\ \text{m}^3/\text{s}$) and ~12 Sv during Heinrich event 1 and the Younger Dryas stadial, respectively. Here we adopt the strategy of combining SST reconstructions with climate model experiments to estimate the magnitude of differences in AMOC strength between MIS3 stadial states and interstadial states. To this end, we use a set of MIS3 freshwater hosing/extraction experiments using the comprehensive coupled Community Climate System Model version 3 (CCSM3) [*Xiao Zhang et al.*, 2014] to construct a global spatial fingerprint of oceanic temperature anomalies in response to AMOC changes. After testing the significance of linear temperature-AMOC regressions, we identify optimal locations for temperature reconstructions for an estimate of MIS3 AMOC variability.

©2015. American Geophysical Union. All Rights Reserved.

2. Model Description and Experimental Design

The Community Climate System Model version 3 (CCSM3) is a global coupled general circulation model (CGCM) consisting of the four components: atmosphere, land, ocean, and sea ice [*Collins et al*., 2006; *Yeager et al*., 2006]. We use the atmospheric component (Community Atmosphere Model version 3) with T31 horizontal resolution (3.75° transform grid) and 26 levels in the vertical. The Community Land Model (version 3) has the same horizontal resolution as the atmosphere and contains 10 subsurface soil levels. New parametrizations of canopy interception and soil evaporation have been applied to the land model [*Oleson et al*., 2008], and the Dynamic Global Vegetation Model [*Levis et al*., 2004] was activated in our simulations [cf. *Handiani et al*., 2013; *Mohtadi et al*., 2014]. The ocean component (Parallel Ocean Program) has 25 layers with layer thickness increasing from 8 m at the surface to around 500 m at the ocean bottom. The nominal horizontal resolution is 3° with latitudinal grid refinement of 0.9° around the equator and the North Pole displaced over Greenland [cf. *Smith et al*., 1995]. The Community Sea Ice Model shares the same horizontal resolution with the ocean component.

A MIS3 baseline simulation centered at 38 ka B.P. (time slice right in the middle of a rather regular sequence of D-O cycles) was performed with 38 ka B.P. orbital forcing [*Berger*, 1978], corresponding greenhouse gas concentrations of CO_2 (215 ppmv), CH_4 (501 ppbv), and N_2O (234 ppbv) [*Flückiger et al*., 2004; *Spahni et al*., 2005; *Ahn and Brook*, 2007; *Bereiter et al*., 2012], the 38 ka B.P. ICE-5G continental ice sheet distribution [*Peltier*, 2004], as well as a correspondingly modified land-sea distribution (e.g., closed Bering Strait due to a reduced sea level). Under these boundary conditions, 12 freshwater hosing/extraction experiments were carried out which all branched off from the equilibrated MIS3 baseline simulation [*Xiao Zhang et al*., 2014]. Different rates of continuous, unbalanced surface freshwater fluxes (homogeneously distributed over the Nordic Seas and treated as virtual salinity fluxes) [e.g., *Prange and Gerdes*, 2006], ranging from ± 0.005 Sv to ± 0.2 Sv (±0.005 Sv, ±0.01 Sv, ±0.02 Sv, ±0.04 Sv, ±0.1 Sv, and ±0.2 Sv), were applied in these hosing (positive freshwater flux into the ocean) and extraction (negative freshwater flux) experiments.

Integration times were 500–550 years for each hosing/extraction experiment. For further details on the initialization of model simulations and integration lengths, the reader is referred to *Xiao Zhang et al*. [2014]. Analyses of the 13 (quasi-)equilibrium states are based on the last 100 year mean climatologies of each experiment.

3. AMOC Response to Freshwater Forcing

In the 38 ka B.P. baseline run, the strength of the AMOC (defined as the maximum of the meridional stream function below 300 m in the North Atlantic Ocean) is around 15.4 Sv, which is ~1.5 Sv stronger than in a modern (preindustrial) control run, with a southward flow of North Atlantic deep water occurring at shallower levels compared to modern [*Xiao Zhang et al*., 2014]. The inflow of warm and salty Atlantic water from the south keeps large parts of the Nordic Seas ice free and maintains convection and deep water formation during winter. The MIS3 baseline state is very sensitive with respect to minor freshwater perturbations. The AMOC equilibrium response to freshwater forcing in our set of experiments reveals the existence of a threshold by an abrupt drop in AMOC strength for North Atlantic freshwater forcing between −0.02 Sv and +0.02 Sv. A decrease to ~11 Sv of the AMOC strength in response to a weak positive freshwater forcing of 0.02 Sv was simulated. In contrast, AMOC strength increases to ~17 Sv upon a negative forcing of 0.02 Sv. The surface air temperature difference in central Greenland between these two climate states is about 8 K in the annual mean [*Xiao Zhang et al*., 2014]. With the maximum freshwater forcing in our experiments of +0.2 Sv, the AMOC drops to 4.9 Sv within ~150 model years. We note that this magnitude of freshwater forcing is consistent with estimates of the order of magnitude of meltwater influx during Heinrich stadials [*Hemming*, 2004].

4. Ocean Equilibrium Temperature Response to AMOC Changes

Relative to the 38 ka B.P. baseline experiment, SST anomalies exhibit a bipolar seesaw pattern in all freshwater hosing (extraction) experiments, featuring a general cooling (warming) in the Northern Hemisphere and a warming (cooling) in the Southern Hemisphere due to a reduced (enhanced) northward heat transport in the

©2015. American Geophysical Union. All Rights Reserved.

Atlantic Ocean [*Crowley*, 1992; *Stocker and Johnsen*, 2003]. We determine the global fingerprint of ocean temperature anomalies in response to AMOC changes by linear least squares regression analysis using the 13 MIS3 equilibrium climate states. Significance of the linear temperature-AMOC (i.e., temperature on AMOC) regressions is tested by an ANOVA (analysis of variance) *F* test [e.g., *Li*, 1964; *Davis*, 1986].

At the surface, the strongest response (i.e., the largest regression coefficient or slope) occurs in the northeastern North Atlantic (Figure 1a; annual mean). Here SST increases more strongly with increasing AMOC strength than in any other region of the Northern Hemisphere. The signal is advected toward the tropics along the eastern margin of the North Atlantic via the Canary Current as already described in earlier freshwater hosing model studies [e.g., *Lohmann*, 2003; *Prange et al*., 2004]. Despite the use of different models and boundary conditions, maximum sensitivities of SST upon AMOC change in the northern North Atlantic and along the eastern North Atlantic margin have also been found in previous studies [e.g., *Heslop and Paul*, 2012; *Ritz et al*., 2013].

During boreal summer, the SST sensitivity to AMOC change is even larger in the northern North Atlantic region than in the annual mean (Figure 1b), which can mainly be attributed to sea ice effects in winter. For a weak AMOC (i.e., smaller than ~11 Sv), large areas in the northern North Atlantic are ice covered in winter [*Xiao Zhang et al*., 2014] such that further reduction in AMOC strength does not lead to further sea surface cooling once the freezing point is reached. This leads to a smaller SST-AMOC regression slope in winter and, hence, in the annual mean. Apart from the North Atlantic realm, differences between the annual mean and the boreal summer SST response are small (Figures 1a and 1b). For instance, in both cases the zero line of the regression slope (i.e., the "seesaw's fulcrum") resides between 10°N and 20°N in the eastern North Atlantic, consistent with proxy evidence [*Zarriess et al*., 2011].

At subsurface levels the ocean temperature response pattern to AMOC changes is very different compared to the surface. As an example, Figure 1c shows the linear regression coefficients at 300 m depth. Except for the subtropical North Atlantic region, where the subsurface temperature response resembles the surface signal due to advection of water masses from the northeastern North Atlantic by the subtropical gyre, subsurface temperatures decrease (increase) with increasing (decreasing) AMOC strength everywhere in the Atlantic Ocean. Subsurface and deep ocean warming in response to past AMOC slowdowns is evidenced by several proxy records from the Atlantic realm [*Rasmussen and Thomsen*, 2004; *Rühlemann et al*., 2004; *Lopes dos Santos et al*., 2010; *Marcott et al*., 2011; *Schmidt et al*., 2012]. In the northern North Atlantic/Nordic Seas, the subsurface warming can be attributed to heat accumulation in these ocean layers as vertical mixing by convection is reduced or even shut down. The subsurface signal is transmitted globally due to a global thermocline adjustment by baroclinic waves [*Huang et al*., 2000; *Goodman*, 2001; *Cessi et al*., 2004; *Zhang et al*., 2012], though the subsurface temperature response becomes relatively small in the Pacific Ocean. We note that subsurface warming in high northern latitudes during stadials has been suggested to destabilize adjacent ice shelves and, thus, to trigger ice stream surges producing Heinrich events [*Marcott et al*., 2011; *Shaffer et al*., 2004; *Álvarez-Solas et al*., 2011].

5. Estimating the Magnitude of AMOC Variations During MIS3

Having constructed the spatial fingerprint of ocean temperature anomalies with respect to AMOC changes, we attempt to estimate the magnitude of AMOC variations during MIS3 using SST reconstructions from sites of highest temperature sensitivities (i.e., largest regression slopes) to AMOC changes. Apart from being obtained in regions of highest SST sensitivity, the proxy records need to cover a substantial part of MIS3 (with a sufficient number of stadial and interstadial intervals for a reasonable statistical analysis) and must be of sufficiently high resolution such that D-O stadials and interstadials can unambiguously be identified and are captured by several data points each.

We identified four high-resolution records that fulfill the required criteria, clearly showing D-O cycles during MIS3 in annual mean or summer temperature from the highly sensitive northern/northeastern Atlantic region (Figure 1a): Irminger Sea core SO82-5 (summer SST derived from planktic foraminiferal assemblages using Similarity Maximum Modern-Analog Technique (SIMMAX) modern analog technique transfer function; SIMMAX is an acronym for a modern analog technique using a similarity index) [*van Kreveld et al*., 2000], northeast Atlantic (eastern Rockall Trough) core MD95-2006 (summer SST derived from planktic foraminiferal assemblage counts using artificial neural network technique) [*Dickson et al*., 2008], Iberian

©2015. American Geophysical Union. All Rights Reserved.

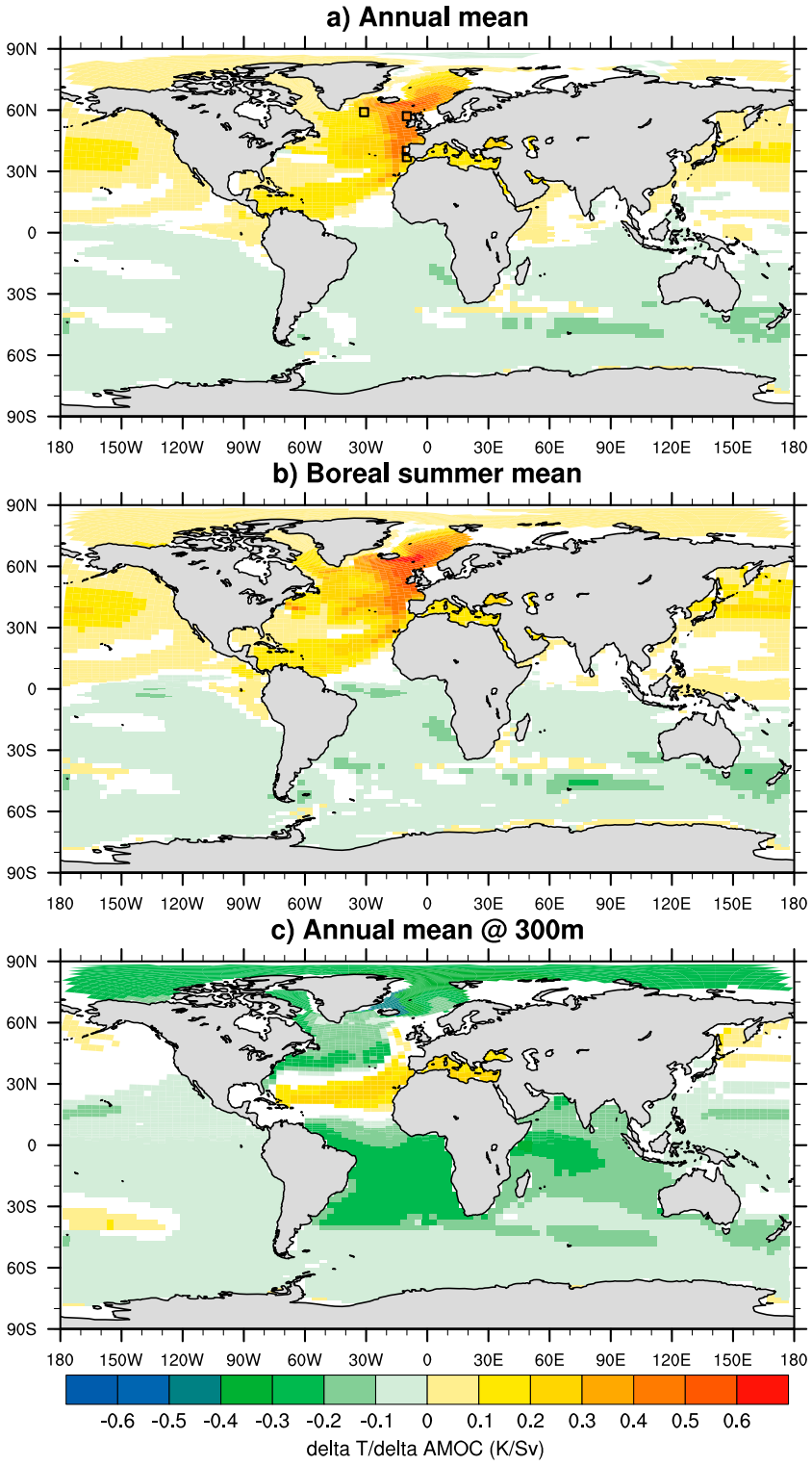

Figure 1. Ocean temperature changes in response to changes in annual mean AMOC strength as given by the least squares regression slopes calculated from the equilibrium states of the set of MIS3 freshwater hosing/extraction experiments for (a) annual mean SST, (b) boreal summer (June-July-August; JJA) SST, and (c) 300 m depth annual mean. Locations which do not show significant ($p < 0.05$) linear temperature-AMOC regression according to an ANOVA F test are white. Frames in Figure 1a show the locations of marine sediment cores providing high-resolution MIS3 temperature reconstructions (see text; Table 1).

©2015. American Geophysical Union. All Rights Reserved.

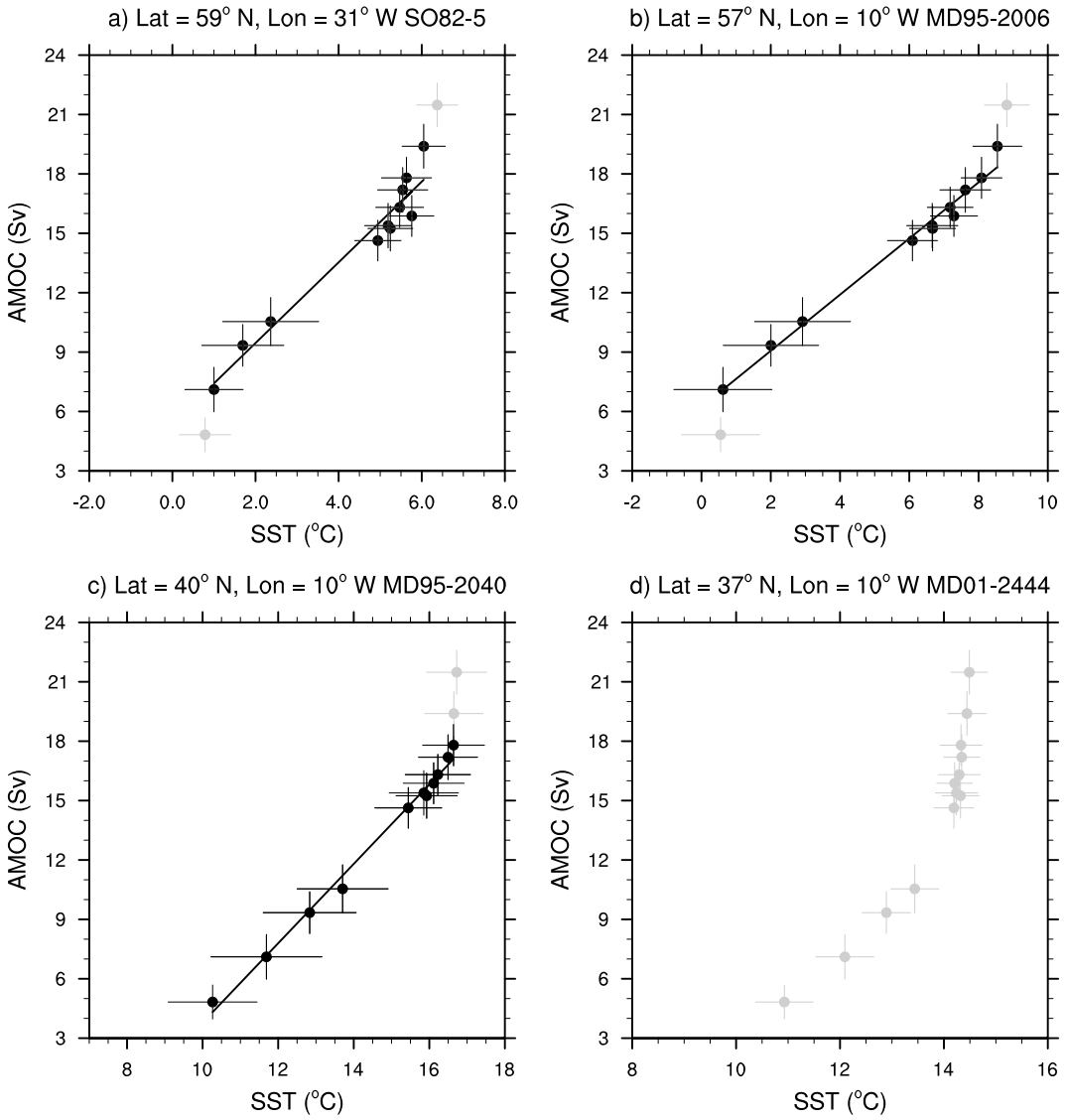

Figure 2. Annual mean AMOC strength versus annual mean or summer (JJA) SST at the four selected sediment core locations (Figure 1) as given by the set of equilibrium states of the MIS3 freshwater hosing/extraction experiments along with linear regression lines. States marked by gray points were excluded from the linear regression analysis. (a) Summer SST in the Irminger Sea (SO82-5), (b) summer SST in the Northeast Atlantic (MD95-2006), (c) summer SST at the Iberian margin (MD95-2040), and (d) annual mean SST at the Iberian margin (MD01-2444). Due to its highly nonlinear behavior, the AMOC-SST relationship at site MD01-2444 was not considered in the estimation of MIS3 AMOC variation. Model SSTs are taken from the nearest single grid point to the corresponding core location. All values are based on 100 year means. Bars show the standard deviations calculated from annual or summer, respectively, values over 100 model years.

margin core MD95-2040 (summer SST derived from planktic foraminiferal assemblages using SIMMAX modern analog technique) [*de Abreu et al.*, 2003], and Iberian margin core MD01-2444 (annual mean SST based on alkenone unsaturation index $U^{k'}_{37}$) [*Martrat et al.*, 2007]. All SST records cover the entire MIS3 except for the record of MD95-2006 which only covers the interval 56–40 ka B.P.

Estimating the magnitude of AMOC variations using reconstructed SST changes further requires linearity of the AMOC-SST relationship (i.e., the SST sensitivity must be independent of the AMOC state) [cf. *Heslop and Paul*, 2012]. Figure 2 shows the modeled AMOC-SST relationships at the four core locations. Considering the small amount of data points, linearity is assessed by visual inspection only. For extremely strong AMOC states (>19–20 Sv) linearity of the AMOC-SST relation visibly disappears at all cores locations, whereas linearity disappears for very weak AMOC (<5 Sv) at core locations SO82-5 and MD95-2006. In between, the

©2015. American Geophysical Union. All Rights Reserved.

Table 1. Estimated Summer SST Differences Between MIS3 Interstadial and (Non-Heinrich) Stadial States at the Three Selected North Atlantic Core Locations From Paleothermometry, Slope of Least Squares Linear Regression of AMOC on Summer SST as Derived From the Equilibrium States of the Set of MIS3 Freshwater Hosing/Extraction Model Experiments (Figure 2), and Estimated AMOC Variations With Uncertainties (1σ) Following From Gaussian Uncertainty Propagation

Sediment Core Number and Location	Estimated SST Difference Between Interstadial and Stadial States From the Sediment Core (°C)	Modeled Slope of AMOC-SST Regression (Sv/°C)	Estimated AMOC Difference Between Interstadial and Stadial States (Sv)
SO82-5 (59°N, 31°W; Irminger Sea)	4.5 ± 1.3 (summer)	2.0 ± 0.2	9.3 ± 2.7
MD95-2006 (57°N, 10°W; Northeast Atlantic)	6.3 ± 1.0 (summer)	1.4 ± 0.1	8.9 ± 1.5
MD95-2040 (40°N, 10°W; Iberian margin)	5.3 ± 1.6 (summer)	2.0 ± 0.1	10.6 ± 3.2

AMOC-SST relationship is sufficiently linear, except for site MD01-2444, which shows a highly nonlinear behavior throughout. We therefore decided to remove the temperature record of MD01-2444 as well as the extreme AMOC states (marked in gray, Figure 2) from the linear regression analysis and considered only the linear AMOC-SST regimes at the three remaining sites (SO82-5, MD95-2006, and MD95-2040). This implies that the following estimation of stadial-interstadial AMOC changes requires interstadial AMOC strength of less than ~19 Sv during MIS3.

For each record (SO82-5, MD95-2006, and MD95-2040), we estimated a mean stadial SST and a mean interstadial SST by taking all stadial and interstadial states in the time interval 50 ka to 30 ka B.P. into account (for the MD95-2006 record, the shorter interval 50–40 ka B.P. was used which still provides five D-O stadial-interstadial transitions). Uncertainties in these temperature estimates and stadial-interstadial diversity were taken into account by calculating the standard deviations of the sets of individual stadial and interstadial temperature estimates for each record. The calculated differences between mean interstadial and mean stadial SSTs along with 1σ uncertainties for each record are listed in Table 1. Note that we excluded Heinrich stadials [*Hemming*, 2004] from our estimates of mean stadial temperatures due to their infrequent occurrence and hence poor statistics (only Heinrich events 4 and 5 occur in the interval 50–30 ka B.P.).

Using the linearized AMOC-SST relationships (i.e., regression of AMOC on SST) from the CCSM3 experiments at the locations of the three sediment core sites SO82-5, MD95-2006, and MD95-2040 (Figure 2), we estimate the magnitude of AMOC changes associated with stadial-interstadial SST differences derived from the proxy records. Table 1 summarizes the calculated regression slopes and resulting estimates for AMOC changes along with 1σ uncertainties following from Gaussian uncertainty propagation. All three estimates are around 9–10 Sv. Calculating a weighted mean from the three AMOC estimates and their 1σ uncertainties yields a 9.2 ± 1.2 Sv mean difference of the AMOC strength between interstadial and (non-Heinrich) stadial states during MIS3. The highly nonlinear response of AMOC strength to freshwater forcing [*Xiao Zhang et al.*, 2014] further implies that the stadial AMOC was likely weaker than 11 Sv, while the interstadial AMOC was likely stronger than 14 Sv, according to the CCSM3 results (Figure 2).

Our estimates are based on AMOC-SST regression analyses of (quasi-)equilibrium climate states. However, D-O stadials and interstadials are transient phenomena and sometimes do not persist longer than a few hundred years [cf. *Dickson et al.*, 2008]. It is therefore instructive to examine the timescale of SST adjustment (i.e., transient behavior) to AMOC changes at the core sites. Figure 3 shows the SST and AMOC spin-up time series for the two experiments with extreme forcing, i.e., +0.2 Sv (Figure 3a) and −0.2 Sv (Figure 3b) freshwater forcing. All time series demonstrate a rapid adjustment of SST to AMOC changes at the core sites on a shorter-than-century timescale. The rapid SST response at the core locations lends support to our equilibrium climate approach to estimate stadial-interstadial AMOC variations using North Atlantic records rather than records from southern latitudes where temperature adjustment to AMOC change may take much longer [e.g., *Schmittner et al.*, 2003; *Knutti et al.*, 2004].

Although there is evidence from records of ice-rafted debris for enhanced iceberg and, hence, freshwater fluxes into the Nordic Seas during D-O stadials [e.g., *Dokken and Jansen*, 1999; *van Kreveld et al.*, 2000; *Elliot et al.*, 2002], we note that other potential forcing mechanisms for D-O climate transitions may exist and have been discussed in the literature [e.g., *Xu Zhang et al.*, 2014; *Peltier and Vettoretti*, 2014, and references therein]. Independent of the real D-O trigger mechanism, freshwater forcing in the present study can be considered a pragmatic way of creating a set of different climate states.

©2015. American Geophysical Union. All Rights Reserved.

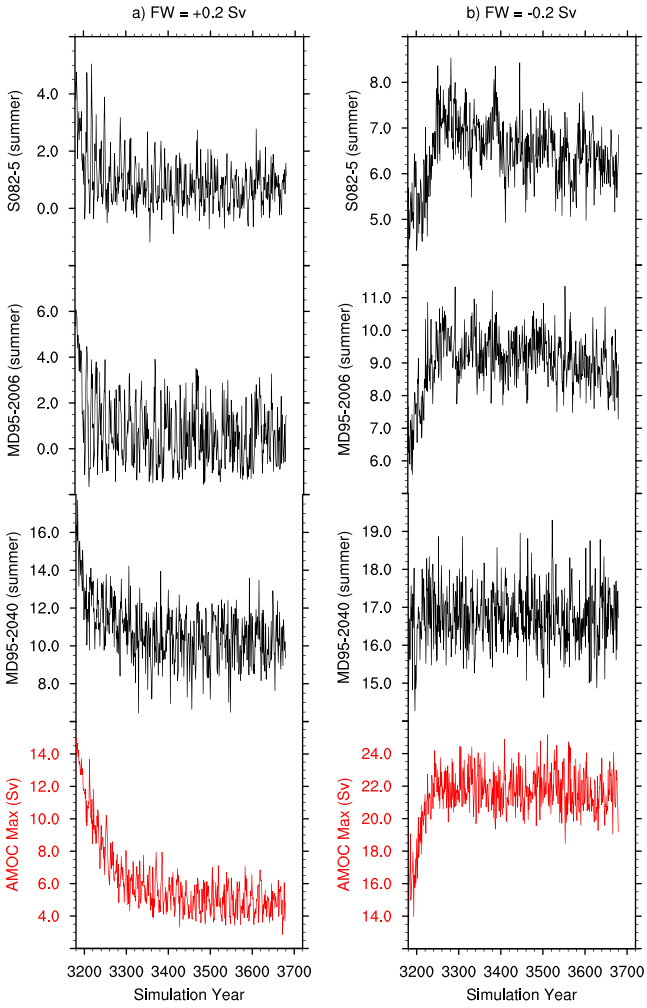

Figure 3. Time series of summer (JJA) SST at the three selected sediment core locations (see Table 1) along with annual mean AMOC strength (red) in (a) the +0.2 Sv freshwater hosing run and (b) the −0.2 Sv freshwater extraction run. Both experiments start at model year 3170 (from the equilibrated MIS3 baseline run) and are integrated for 500 years each with continuous positive/negative freshwater forcing. Core numbers are indicated on the left.

Keeping atmospheric greenhouse gas concentrations fixed in our simulations, our approach of SST-based estimates of AMOC variability neglects potential feedbacks associated with changes in atmospheric greenhouse gas concentrations and, hence, longwave radiative forcing caused by ocean circulation changes [e.g., *Schmittner and Galbraith*, 2008]. However, the small CO_2 variations associated with non-Heinrich stadials and the following D-O warming events are ~5 ppm or less [*Ahn and Brook*, 2014] and have no noticeable effect (i.e., less than 1 K) on northeast Atlantic SST [*Van Meerbeeck et al.*, 2009]. It is therefore reasonable to assume that the first-order effect of MIS3 millennial-scale AMOC variability on North Atlantic temperatures is directly due to changes in the large-scale oceanic heat transport.

6. Conclusions

We have investigated the ocean temperature response to variations in AMOC strength by performing a set of freshwater hosing/extraction experiments under MIS3 (38 ka B.P.) glacial boundary conditions using the comprehensive coupled climate model CCSM3. The main target of this study was to provide a global spatial fingerprint of ocean temperature response to D-O-related AMOC changes and, further, to estimate the differences in AMOC strength between MIS3 stadial and interstadial states by combining temperature reconstructions with model simulations. The simulations suggest the highest SST sensitivity to AMOC changes in the northeastern North Atlantic, especially in summer. Due to the high sensitivity and a rapid adjustment time, SST reconstructions from this region turn out to be particularly suitable for estimating past AMOC changes. Significant temperature responses are also found at subsurface levels. However, the subsurface temperature fingerprint could not be exploited for our purpose of estimating MIS3 AMOC variability due to a lack of high-resolution D-O-resolving subsurface temperature records.

From three North Atlantic SST records, we could estimate a mean stadial-interstadial AMOC strength difference of 9.2 ± 1.2 Sv (Heinrich stadials excluded), provided that interstadial AMOC strength was below ~19 Sv during MIS3. Moreover, the CCSM3 results suggest that the stadial AMOC was weaker than 11 Sv, while the interstadial AMOC was stronger than 14 Sv. These estimates are based on one CGCM only. Besides the need for more high-resolution surface and subsurface proxy records for the MIS3 interval, more MIS3 simulations using state-of-the-art CGCMs are needed to better constrain this estimate. So far, only few CGCM simulations of MIS3 climate exist [*Merkel et al.*, 2010; *Singarayer and Valdes*, 2010; *Brandefelt et al.*, 2011; *Gong et al.*, 2013; *Mohtadi et al.*, 2014]. Sophisticated data assimilation techniques could provide absolute numbers for AMOC strength [cf. *Kurahashi-Nakamura et al.*, 2014], but for MIS3, this would require a much larger glacial proxy database.

©2015. American Geophysical Union. All Rights Reserved.

Acknowledgments
This study was funded by the DFG-Research Center/Cluster of Excellence "The Ocean in the Earth System." The CCSM3 climate model experiments were run on the SGI Altix Supercomputer of the "Norddeutscher Verbund für Hoch- und Höchstleistungsrechnen" (HLRN). We thank two anonymous reviewers for their constructive comments and suggestions.

The Editor thanks two anonymous reviewers for their assistance in evaluating this paper.

References

Ahn, J., and E. J. Brook (2007), Atmospheric CO_2 and climate from 65 to 39 ka B.P., *Geophys. Res. Lett.*, *34*, L10703, doi:10.1029/2007GL029551.
Ahn, J., and E. J. Brook (2014), Siple Dome ice reveals two modes of millennial CO_2 change during the last ice age, *Nat. Commun.*, *5*, 3723, doi:10.1038/ncomms4723.
Álvarez-Solas, J., M. Montoya, C. Ritz, G. Ramstein, S. Charbit, C. Dumas, K. Nisancioglu, T. Dokken, and A. Ganopolski (2011), Heinrich event 1: An example of dynamical ice-sheet reaction to oceanic changes, *Clim. Past*, *7*, 1297–1306.
Bereiter, B., et al. (2012), Mode change of millennial CO_2 variability during the last glacial cycle associated with a bipolar marine carbon seesaw, *Proc. Natl. Acad. Sci. U.S.A.*, *109*, 9755–9760.
Berger, A. (1978), Long term variations of daily insolation and Quaternary climatic changes, *J. Atmos. Sci.*, *35*, 2362–2367.
Bond, G., W. Broecker, S. Johnsen, J. McManus, L. Labeyrie, J. Jouzel, and G. Bonani (1993), Correlations between climate records from North Atlantic sediments and Greenland ice, *Nature*, *365*, 143–147.
Brandefelt, J., E. Kjellström, J.-O. Näslund, G. Strandberg, A. H. L. Voelker, and B. Wohlfarth (2011), A coupled climate model simulation of marine isotope stage 3 stadial climate, *Clim. Past*, *7*, 649–670.
Broecker, B., et al. (1992), Evidence for massive discharges of icebergs into the North Atlantic Ocean during the last glacial period, *Nature*, *360*, 245–249.
Broecker, W. S. (2000), Abrupt climate change: Causal constraints provided by the paleoclimate record, *Earth Sci. Rev.*, *51*, 137–154.
Cessi, P., K. Bryan, and R. Zhang (2004), Global seiching of thermocline waters between the Atlantic and the Indian–Pacific Ocean Basins, *Geophys. Res. Lett.*, *31*, L04302, doi:10.1029/2003GL019091.
Collins, W. D., et al. (2006), The Community Climate System Model Version 3 (CCSM3), *J. Clim.*, *19*, 2122–2143.
Crowley, T. J. (1992), North Atlantic deep water cools the Southern Hemisphere, *Paleoceanography*, *7*, 489–497, doi:10.1029/92PA01058.
Dansgaard, W., et al. (1993), Evidence for general instability of past climate from a 250-kyr ice-core record, *Nature*, *364*, 218–220.
Davis, J. C. (1986), *Statistics and Data Analysis in Geology*, 2nd ed., 646 pp., John Wiley, New York.
de Abreu, L., N. J. Shackleton, J. Schönfeld, M. Hall, and M. Chapman (2003), Millennial-scale oceanic climate variability off the Western Iberian margin during the last two glacial periods, *Mar. Geol.*, *196*, 1–20.
Dickson, A. J., W. E. N. Austin, I. R. Hall, M. A. Maslin, and M. Kucera (2008), Centennial-scale evolution of Dansgaard-Oeschger events in the northeast Atlantic Ocean between 39.5 and 56.5 ka B.P., *Paleoceanography*, *23*, PA3206, doi:10.1029/2008PA001595.
Dokken, T. M., and E. Jansen (1999), Rapid changes in the mechanism of ocean convection during the last glacial period, *Nature*, *401*, 458–461.
Elliot, M. L., L. Labeyrie, and J. C. Duplessy (2002), Changes in North Atlantic deep-water formation associated with the Dansgaard-Oeschger temperature oscillations (60–10 ka), *Quat. Sci. Rev.*, *21*, 1153–1165.
EPICA Community Members (2006), One-to-one coupling of glacial climate variability in Greenland and Antarctica, *Nature*, *444*, 195–198.
Flückiger, J., T. Blunier, B. Stauffer, J.r. Chappellaz, R. Spahni, K. Kawamura, J. Schwander, T. F. Stocker, and D. Dahl-Jensen (2004), N_2O and CH_4 variations during the last glacial epoch: Insight into global processes, *Global Biogeochem. Cycles*, *18*, GB1020, doi:10.1029/2003GB002122.
Ganachaud, A., and C. Wunsch (2000), Improved estimates of global ocean circulation, heat transport and mixing from hydrographic data, *Nature*, *408*, 453–457.
Gebbie, G., and P. Huybers (2006), Meridional circulation during the Last Glacial Maximum explored through a combination of South Atlantic $\delta^{18}O$ observations and a geostrophic inverse model, *Geochem. Geophys. Geosyst.*, *7*, Q11N07, doi:10.1029/2006GC001383.
Gong, X., G. Knorr, and G. Lohmann (2013), Dependence of abrupt Atlantic meridional ocean circulation changes on climate background states, *Geophys. Res. Lett.*, *40*, 3691–3704, doi:10.1002/grl.50701.
Goodman, P. J. (2001), Thermohaline adjustment and advection in an OGCM, *J. Phys. Oceanogr.*, *31*, 1477–1497, doi:10.1175/1520-0485(2001)031.
Grousset, F. E., et al. (1993), Patterns of ice-rafted detritus in the glacial North Atlantic, *Paleoceanography*, *8*, 175–192, doi:10.1029/92PA02923.
Handiani, D., A. Paul, M. Prange, U. Merkel, L. Dupont, and X. Zhang (2013), Tropical vegetation response to Heinrich Event 1 as simulated with the UVic ESCM and CCSM3, *Clim. Past*, *9*, 1683–1696, doi:10.5194/cp-9-1683-2013.
Hemming, S. R. (2004), Heinrich events: massive late Pleistocene detritus layers of the North Atlantic and their global climate imprint, *Rev. Geophys.*, *42*, RG1005, doi:10.1029/2003RG000128.
Heslop, D., and A. Paul (2012), Fingerprinting of the Atlantic Meridional Overturning Circulation in climate models to aid in the design of proxy investigations, *Clim. Dyn.*, *38*, 1047–1064, doi:10.1007/s00382-011-1042-0.
Huang, R. X., M. A. Cane, N. Naik, and P. Goodman (2000), Global adjustment of the thermocline in response to deepwater formation, *Geophys. Res. Lett.*, *27*, 759–762, doi:10.1029/1999GL002365.
Johns, W. E., et al. (2011), Continuous, array-based estimates of Atlantic Ocean heat transport at 26.5°N, *J. Clim.*, *24*, 2429–2449.
Keigwin, L. D., and E. A. Boyle (1999), Surface and deep ocean variability in the northern Sargasso Sea during marine isotope stage 3, *Paleoceanography*, *14*(2), 164–170, doi:10.1029/1998PA900026.
Knutti, R., J. Flückiger, T. F. Stocker, and A. Timmermann (2004), Strong hemispheric coupling of glacial climate through freshwater discharge and ocean circulation, *Nature*, *430*, 851–856.
Kurahashi-Nakamura, T., M. Losch, and A. Paul (2014), Can sparse proxy data constrain the strength of the Atlantic meridional overturning circulation?, *Geosci. Model Dev.*, *7*, 419–432.
LeGrand, P., and C. Wunsch (1995), Constraints from paleo-tracer data on the North Atlantic circulation during the Last Glacial Maximum, *Paleoceanography*, *10*, 1011–1045, doi:10.1029/95PA01455.
Levis, S., et al. (2004), The community land model's dynamic global vegetation model (CLM-DGVM): Technical description and user's guide, *Tech. Note NCAR/TN-459+STR*, 50 pp., Natl. Cent. for Atmos. Res., Boulder, Colo.
Li, C. C. (1964), *Introduction to Experimental Statistics*, McGraw-Hill, New York.
Lohmann, G. (2003), Atmospheric and oceanic freshwater transport during weak Atlantic overturning circulation, *Tellus*, *55*, 438–449.
Lopes dos Santos, R. A., et al. (2010), Glacial interglacial variability in Atlantic meridional overturning circulation and thermocline adjustments in the tropical North Atlantic, *Earth Planet. Sci. Lett.*, *300*, 407–414.
Lynch-Stieglitz, J., et al. (2007), Atlantic Meridional Overturning Circulation during the Last Glacial Maximum, *Science*, *316*, 66–69.
Marcott, S. A., et al. (2011), Ice-shelf collapse from subsurface warming as trigger for Heinrich events, *Proc. Natl. Acad. Sci. U.S.A.*, *108*, 13,415–13,419, doi:10.1073/pnas.1104772108.
Martrat, B., J. O. Grimalt, N. J. Shackleton, L. de Abreu, M. A. Hutterli, and T. F. Stocker (2007), Four climate cycles of recurring deep and surface water destabilizations on the Iberian Margin, *Science*, *317*, 502–507.
McManus, J. F., R. Francois, J.-M. Gherardi, L. D. Keigwin, and S. Brown-Leger (2004), Collapse and rapid resumption of Atlantic meridional circulation linked to deglacial climate changes, *Nature*, *428*, 834–837.

©2015. American Geophysical Union. All Rights Reserved.

Merkel, U., M. Prange, and M. Schulz (2010), ENSO variability and teleconnections during glacial climates, *Quat. Sci. Rev.*, *29*, 86–100.
Mohtadi M., M. Prange, Delia W. Oppo, R. De Pol-Holz, U. Merkel, X. Zhang, S. Steinke, and A. Lückge (2014), North Atlantic forcing of tropical Indian Ocean climate, *Nature*, *509*, 76–80.
Oleson, K. W., et al. (2008), Improvements to the Community Land Model and their impact on the hydrological cycle, *J. Geophys. Res.*, *113*, G01021, doi:10.1029/2007JG000563.
Peltier, W. R. (2004), Global glacial isostasy and the surface of the ice-age Earth: The ICE-5G (VM2) model and GRACE, *Annu. Rev. Earth Planet. Sci.*, *32*, 111–149.
Peltier, W. R., and G. Vettoretti (2014), Dansgaard-Oeschger oscillations predicted in a comprehensive model of glacial climate: A "kicked" salt oscillator in the Atlantic, *Geophys. Res. Lett.*, *41*, 7306–7313, doi:10.1002/2014GL061413.
Prange, M., and R. Gerdes (2006), The role of surface freshwater flux boundary conditions in Arctic Ocean modelling, *Ocean Modelling*, *13*, 25–43.
Prange, M., G. Lohmann, V. Romanova, and M. Butzin (2004), Modelling tempo-spatial signatures of Heinrich Events: Influence of the climatic background state, *Quat. Sci. Rev.*, *23*, 521–527.
Rahmstorf, S. (2002), Ocean circulation and climate during the past 120,000 years, *Nature*, *419*, 207–214.
Rasmussen, T. L., and E. Thomsen (2004), The role of the North Atlantic Drift in the millennial timescale glacial climate fluctuations, *Palaeogeogr. Palaeoclimatol. Palaeoecol.*, *210*, 101–116.
Ritz, S. P., F. T. Stocker, J. O. Grimalt, L. Menviel, and A. Timmermann (2013), Estimated strength of the Atlantic overturning circulation during the last deglaciation, *Nat. Geosci.*, *6*, 208–212.
Rühlemann, C., G. Lohmann, A. Paul, M. Prange, and G. Wefer (2004), Intermediate depth warming in the tropical Atlantic related to weakened thermohaline circulation: Combining paleoclimate and modeling data for the last deglaciation, *Paleoceanography*, *19*, PA1025, doi:10.1029/2003PA000948.
Sarnthein, M., et al. (2001), *Fundamental Modes and Abrupt Changes in North Atlantic Circulation and Climate Over the Last 60 ky—Concepts, Reconstructions and Numerical Modeling, The Northern North Atlantic: A Changing Environment*, edited by P. Schäfer et al., pp. 365–410, Springer, New York.
Schmidt, M. W., P. Chang, J. E. Hertzberg, T. R. Them II, J. Link, and B. L. Otto-Bliesner (2012), Impact of abrupt deglacial climate change on tropical Atlantic subsurface temperatures, *Proc. Natl. Acad. Sci. U.S.A.*, *109*, 14,348–14,352.
Schmittner, A., and E. D. Galbraith (2008), Glacial greenhouse gas fluctuations controlled by ocean circulation changes, *Nature*, *456*, 373–376, doi:10.1038/nature07531.
Schmittner, A., O. A. Saenko, and A. J. Weaver (2003), Coupling of the hemispheres in observations and simulations of glacial climate change, *Quat. Sci. Rev.*, *22*, 659–671.
Shaffer, G., S. O. Malskaer, and C. J. Bjerrum (2004), Ocean subsurface warming as a mechanism for coupling Dansgaard-Oeschger climate cycles and ice-rafting events, *Geophys. Res. Lett.*, *31*, L24202, doi:10.1029/2004GL020968.
Singarayer, J. S., and P. J. Valdes (2010), High-latitude climate sensitivity to ice-sheet forcing over the last 120 kyr, *Quat. Sci. Rev.*, *29*, 43–55.
Smith, R. D., S. Kortas, and B. Meltz, (1995), Curvilinear coordinates for global ocean models, *Tech. Rep. LA-UR-95-1146,* Los Alamos National Laboratory, 50 pp.
Spahni, R., et al. (2005), Atmospheric methane and nitrous oxide of the late Pleistocene from Antarctic ice cores, *Science*, *310*, 1317–1321.
Stocker, T. F., and S. J. Johnsen (2003), A minimum thermodynamic model for the bipolar seesaw, *Paleoceanography*, *18*(4), 1087, doi:10.1029/2003PA000920.
van Kreveld, S., M. Sarnthein, H. Erlenkeuser, P. Grootes, S. Jung, M. J. Nadeau, U. Pflaumann, and A. Voelker (2000), Potential links between surging ice sheets, circulation changes, and the Dansgaard-Oeschger cycles in the Irminger Sea, 60-18 kyr, *Paleoceanography*, *15*, 425–442. doi:10.1029/1999PA000464.
Van Meerbeeck, C. J., H. Renssen, and D. M. Roche (2009), How did Marine Isotope Stage 3 and Last Glacial Maximum climates differ?—Perspectives from equilibrium simulations, *Clim. Past*, *5*, 33–51.
Winguth, A., D. Archer, E. Maier-Reimer, and U. Mikolajewicz (2000), Paleonutrient data analysis of the glacial Atlantic using an adjoint ocean general circulation model, in *Inverse Methods in Global Biogeochemical Cycles*, *Geophys. Monogr. Ser.*, vol. 114, edited by P. Kasibhatla et al., pp. 171–183, AGU, Washington, D. C.
Yeager, S. G., C. A. Shields, W. G. Large, and J. J. Hack (2006), The low-resolution CCSM3, *J. Clim.*, *19*, 2545–2566.
Zarriess, M., H. Johnstone, M. Prange, S. Steph, J. Groeneveld, S. Mulitza, and A. Mackensen (2011), Bipolar seesaw in the northeastern tropical Atlantic during Heinrich stadials, *Geophys. Res. Lett.*, *38*, L04706, doi:10.1029/2010GL046070.
Zhang, X., et al. (2012), Changes in equatorial Pacific thermocline depth in response to Panamanian seaway closure: Insights from a multi-model study, *Earth Planet. Sci. Lett.*, *317–318*, 76–84.
Zhang, X., M. Prange, U. Merkel, and M. Schulz (2014), Instability of the Atlantic overturning circulation during marine isotope stage 3, *Geophys. Res. Lett.*, *41*, 4285–4293, doi:10.1002/2014GL060321.
Zhang, X., G. Lohmann, G. Knorr, and C. Purcell (2014), Abrupt glacial climate shifts controlled by ice sheet changes, *Nature*, *512*, 290–294, doi:10.1038/nature13592.

©2015. American Geophysical Union. All Rights Reserved.